Surface Science 678 (2018) 118–123

Contents lists available at ScienceDirect

Surface Science

journal homepage: www.elsevier.com/locate/susc

Ultrathin silica films on Pd(111): Structure and adsorption properties

Héloïse Tissot[a], Xuefei Weng[a], Philomena Schlexer[b], Gianfranco Pacchioni[b,*], Shamil Shaikhutdinov[a,*], Hans-Joachim Freund[a]

[a] Fritz-Haber Institut der Max-Planck Gesellschaft, Faradayweg 4-6, 14195 Berlin, Germany
[b] Dipartimento di Scienza dei Materiali, Università di Milano-Bicocca, via R. Cozzi 55, 20125 Milano, Italy

ARTICLE INFO

Keywords:
Ultrathin films
Silica
CO adsorption
Infrared spectroscopy
Reactions in confined space

ABSTRACT

We studied the preparation of thin silica films on Pd(111) using low energy electron diffraction (LEED), infrared reflection-absorption spectroscopy (IRAS), and scanning tunneling microscopy (STM). The films grow from the onset as a double-layer (bilayer) silicate and show no long-range ordering as judged by LEED, thus bearing close similarities to the silicate films grown on a Pt(111) support. The results provide further evidence that the principal structure (monolayer vs bilayer) of ultrathin silica films on metal substrates is primarily governed by the affinity of a metal substrate to oxygen. Individual adsorption of CO and D_2 on the prepared films showed that both molecules penetrate through the film and chemisorb on the Pd(111) surface. Density functional theory (DFT) calculations showed that CO bonding on Pd(111) underneath the silica film becomes weaker as compared to the bare Pd(111) surface, but the vibrational frequencies remain unaffected, that is in nice agreement with the experimental results.

1. Introduction

Preparation of thin silica films on metal single crystal surfaces was for many years the subject of interest in the “surface science” community, primarily in attempts to provide a well-defined planar system of silica that could model silica-based catalysts [1,2]. Growth of well-ordered silica films has been reported on Mo(112), Ru(0001), Pt(111), and Pd(100) substrates [1,3–6]. The structural motif of the films is a layer of corner sharing SiO_4 tetrahedra like in sheet silicates [1,7]. These silicate films can be one or two layers in thickness depending on a metal substrate used. In contrast to monolayer films, the bilayer films are weakly bound to a metal surface via dispersive forces. In addition, the bilayer films may exhibit no long-range ordering in the plane parallel to the surface. In this case, the films are considered as a two-dimensional analog of the silica glass [8–10]. The atomic structure of the resulting films seems to depend both on the affinity of a supporting metal towards oxygen and the lattice mismatch between the silicate and the metal surface [5,11].

Adsorption studies on bilayer films revealed that molecules in the gas phase may intercalate the interface between the silica film and the metal surface [12]. Our previous infrared reflection-absorption spectroscopy (IRAS) and temperature programmed desorption (TPD) studies of CO and D_2 adsorption on SiO_2/Ru(0001) [12] showed that the process includes gas permeation through the relatively large pores, adsorption (dissociation) and diffusion of ad-species on the metal surface underneath the film. The intercalation does not destroy the silica film, which remains even intact upon the formation of a RuO_2 oxide film underneath, at high oxygen pressures and temperatures [13]. Although oxygen readily reaches the metal surface and dissociates, the oxidation process and the resulting Ru-oxide film are affected by the silicate film, most likely due to the spatial constraints at the interface. Such chemistry “under cover”, also reported for metal supported graphene layers [14,15], opens up a new playground for a rational design of hybrid materials combining silicate as a robust molecular sieve and a metal support as catalytically active material, with the reaction occurring in confined space provided by the interface.

In this work, we address the preparation of silicate films on Pd(111) and its adsorption properties towards CO and D_2. Palladium shows superior activity in hydrogenation reactions and is more noble as compared to Ru(0001). In addition, Pd(111) has a lattice constant by 0.02 Å shorter than Pt(111), on which non-crystalline bilayer films have only been observed [5]. Such comparison would provide a deeper understanding of the role of a metal substrate on the atomic structure of a silica film and its reaction at the interface. In the course of our studies we have learned that Altman and co-workers studied the growth of silica on Pd(111) for comparison with Pd(100) [16]. The authors found that the silica bilayer starts ordering above 850 K and forms an incommensurate crystalline structure resulted in a Moire pattern. Corroborated by density functional theory (DFT), these results revealed the

* Corresponding authors.
E-mail addresses: gianfranco.pacchioni@unimib.it (G. Pacchioni), shaikhutdinov@fhi-berlin.mpg.de (S. Shaikhutdinov).

https://doi.org/10.1016/j.susc.2018.02.016
Received 12 December 2017; Received in revised form 28 February 2018; Accepted 28 February 2018
Available online 01 March 2018
0039-6028/

complex interplay between strain, doping, and charge-transfer, which determine the structure of metal-supported two-dimensional silicate films.

2. Methods and materials

The experiments were performed in an ultra-high vacuum (UHV) chamber (base pressure below 5×10^{-10} mbar) equipped with a low-energy electron diffraction (LEED, from Specs), a Fourier-transform infrared spectrometer (Bruker 66ivs), and a quadrupole mass-spectrometer (QMS, from Hiden) for TPD measurements. The IRA spectra (resolution 4 cm^{-1}) were recorded using p-polarized light at an 84° grazing angle of incidence. Adsorption of CO (purity grade 5.0) and D_2 (3.0) was performed by backfilling the chamber using an additional cold trap to prevent contaminations. Scanning tunneling microscopy (STM) study was performed in another UHV chamber equipped with LEED and a microscope (from Omicron) operated at room temperature. The images were obtained with electrochemically etched W tips. In both setups, silicon was deposited from a Si rod (99.99%, 2 mm in diameter, from Goodfellow) using an electron beam assisted evaporator (Focus EMT3).

Periodic, spin polarized DFT calculations were performed using the Vienna Ab Initio Simulation Package (VASP 5.2) [17–20]. For the exchange-correlation functional, generalized gradient approximations (GGA) were applied in the Perdew, Burke and Ernzerhof (PBE) formulation [21]. To describe electron-ion interactions, the projector augmented wave (PAW) method was used [22,23]. In geometric structure optimizations, all ions were allowed to relax until forces are smaller than 0.01 eV/Å. The Pd bulk lattice parameters were optimized using a (11 × 11 × 11) Γ-centered K-point grid in the Monkhorst–Pack scheme [24]. Dispersion correction was implemented following Tosoni and Sauer [25]. We used a 5-atomic layer Pd(111) slab, and the top three layers were allowed to relax. A Pd(111) lattice constant of 2.76 Å was computed, which differs less than 2% from the experimental value. The SiO_2-(1 × 1)/Pd(111)-(2 × 2) interface showed the lowest strain (~3.9%) on the silica bilayer as compared to other possible configurations computed, up to SiO_2(5 × 5). We used a (5 × 5 × 1) Γ-centered K-point grid, and wave functions were expanded in the plane wave basis up to a kinetic energy of 400 eV. Adsorption energies (E_{ads}) were calculated as $E_{ads} = E(X/S) - E(X) - E(S)$, where E denotes the total energies of the system (X – adsorbate, S – support). In order to determine the vibrational frequencies, the Hessian matrix was calculated using the finite difference method with 0.02 Å atomic displacements in each Cartesian direction. For the frequency calculations, the topmost Pd layer and all CO molecules were allowed to move.

3. Results and discussion

3.1. Experimental results

To prepare silica films on Pd(111) we followed the same approach as used in our laboratories for Ru(0001) and Pt(111) supports. Silicon was vapor-deposited at 100 K onto an oxygen pre-covered Pd(111) surface and then oxidized in 3×10^{-6} mbar O_2 at elevated temperatures until the films showed sharp phonon bands monitored by IRAS. This typically required temperatures as high as 1000 K. Fig. 1 shows IRA-spectra of the films prepared at 1100 K as a function of the film coverage, which was determined by CO titration of Pd at 90 K (see below). The spectra showing two bands (at 1304 and 698 cm^{-1}) look virtually identical to those obtained on Ru(0001) (1302 and 692 cm^{-1}) [6] and Pt(111) (1294 and 690 cm^{-1})[5] supported films, which are characteristic of the bilayer silicate. Although the bands position slightly (~ 20 cm^{-1}) shift with coverage, their intensity is proportional to the amount of Si deposited. Based on these finding we conclude that the silicate film on Pd(111) grows as a bilayer from the onset, i.e. in the same manner as on Pt(111). This finding fits well the general trend for

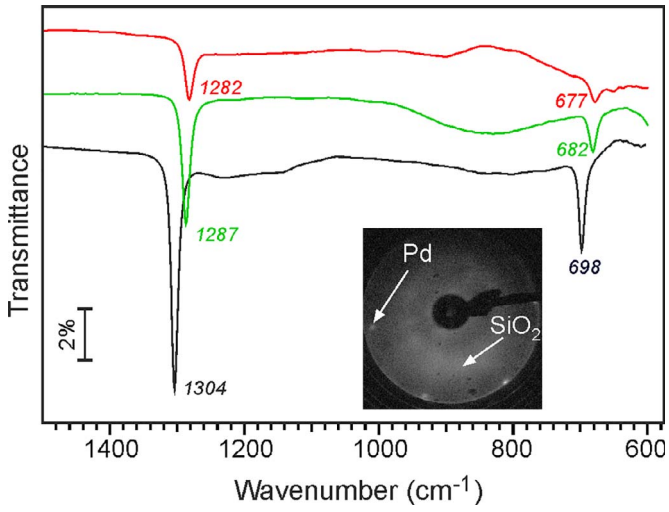

Fig. 1. IRA spectra of silicate films prepared on Pd(111) by oxidation at 1100 K as a function of Si coverage. The bottom (black) line corresponds to the fully covered film. The coverage decreases by factor of 2 and 4 for the green and red lines, respectively. The inset displays a typical LEED pattern where silica overlayer forms a weak (2 × 2) diffraction ring with respect to the Pd(111) spots as indicated. (For interpretation of the references to colour in this figure legend, the reader is referred to the web version of this article.)

the principal structure of a film (bilayer vs monolayer), which is primarily governed by the bond strength in Si-O-metal linkages, and, in turn, correlates with the strength of oxygen binding to the metal surface [5]. Indeed, the heat of oxygen dissociative adsorption on Pd (−170 kJ/mol) is close to that of Pt (−133 kJ/mol), both being well below −220 kJ/mol measured for Ru [26]. Ruthenium may also support a single layer silicate [27], which is the only one formed on Mo (112), showing the highest affinity for oxygen (−544 kJ/mol) among the metal substrates studied [4]. We may, therefore, conclude that ultrathin silicate films on noble metal surfaces will exhibit primarily a bilayer structure.

Although the films show very sharp IRA bands, they did not show a long-range order as judged by LEED. Besides the Pd(111) diffraction spots, only a diffuse (2 × 2) ring was observed (see inset in Fig. 1), which is characteristic of a silicate "glass" film with a broad distribution of silica rings in the surface plane [8,10]. This conclusion is further supported by STM studies performed in another UHV chamber. At submonolayer coverages, silica forms irregularly-shaped islands which coalesce at increasing coverage (Fig. 2). The apparent film thickness (4.3 ± 0.3 Å) is in fair agreement with the geometrical height of a silicate bilayer (see DFT results below). High-resolution images (inset in Fig. 2b) only revealed a short-range periodicity of ~ 6 Å, on average, but no extended domains with a hexagonal, honeycomb-like structure corresponding to the crystalline silicate layer. Therefore, STM results are fully consistent with the IRAS and LEED results showing the formation of an amorphous bilayer silicate film on Pd(111). We believe that the strain caused by the mismatch between the lattice of a free-standing silicate bilayer (= 5.32 Å [28]) and of a Pd(111)-(2 × 2) cell (= 5.50 Å) as well as a lack of strong bonding between Pd and oxygen to form Si-O-Metal linkages, both prevent the formation of a crystalline film. Meanwhile, a Ru(0001) substrate showing a smaller lattice mismatch (5.42 Å for the (2 × 2) structure) and a higher oxygen affinity than of Pt(111) and Pd(111) is better suited to accommodate crystalline structures via monolayer and/or bilayer films.

Although our results generally agree with those reported by Jhang et al. [16] also showing the formation of a bilayer film on Pd(111), none of our films exhibited long-range ordering. We have to recall, however, that on Ru(0001) the bilayer silica films may also form crystalline and amorphous phases (often coexisting) depending on the preparation. Therefore, we cannot exclude that crystalline films may, indeed, be formed on Pd(111) under certain preparation conditions

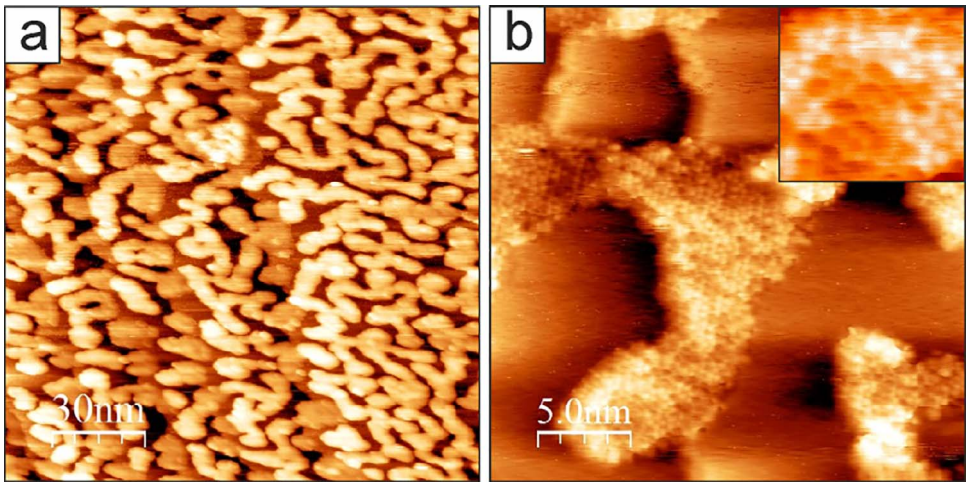

Fig. 2. STM images of a sub-monolayer silica film on Pd(111) prepared at 1050 K. The inset in (b) zoomed in the surface of silica islands. Tunneling bias and current are 2 V and 0.12 nA for all images.

which involve many parameters. In fact, these two studies on Pd(111) reflect the general situation and further exemplify the very complex nature of silica crystallization and the related glass transition.

Next, we studied the adsorption properties of the Pd(111) supported films with respect to CO and D_2. To ensure the films cover the entire crystal surface, the samples were first exposed to low dosages of CO (~ 10 L, 1 L = 10^{-6} Torr sec) at ~ 90 K in order to titrate the Pd(111) surface. Comparison with a CO TPD spectrum obtained on the clean Pd (111) surface revealed only a few percent of the sample area not covered by silica (not shown).

The dense films were then exposed to CO at room temperature at pressures increasing from 1×10^{-7} to 5×10^{-6} mbar and monitored by IRAS (Fig. 3). At low exposures (~ 10 L) no IRA bands were detected. At increasing CO dosage, a broad feature develops at ~1930 cm^{-1}, which gains intensity and shifts to ~ 1935 cm^{-1}. To accelerate CO uptake, the ambient pressure was increased to 10^{-6} mbar. At ~ 200 L of CO, an additional band appears at ~ 2089 cm^{-1}. The two bands grow and apparently saturate at exposures as high as 10^4 L reached by increasing CO pressure to 5×10^{-6} mbar. At saturation, a strong band at 1949 cm^{-1} and a weak signal at 2089 cm^{-1} are observed. This spectrum bears close similarities to the one recorded on the clean Pd(111) surface which is shown in the same panel for comparison. The peaks at 1938 and 2084 cm^{-1} are commonly assigned to CO adsorbing on bridge and on-top sites, respectively [29–31]. As peak positions and their intensities at saturation are almost identical, we conclude that CO fully intercalates the interface between the silicate and the Pd surface. The observed small shifts (by 5–10 cm^{-1}) can tentatively be assigned to the effect of a silicate layer on the CO stretching vibrations (see DFT calculations below) [32].

CO intercalation at the interface is also supported by TPD results as a function of CO exposure at 300 K, shown in Fig. 4. The CO uptake at saturation is almost equal to the one measured on bare Pd(111) (inset in Fig. 4). Apparently, this process is very slow even at room temperature and needs high exposures suggesting that CO permeation most likely occurs through the large silica rings ("pores") and adventitious "holes" in the film. However, the TPD spectra also revealed some differences between the pristine and silica covered surfaces, although CO desorption occurs in the same temperature range. The spectra for SiO_2/Pd (111) correspond to the observed desorption signal at ~405 K which shifts to ~425 K at increasing CO coverage. It is well known [31] that CO on the Pd(111) surface first desorbs from the most weakly bound, on-top sites and subsequently from the bridge sites (at T < 400 K). The remaining CO molecules occupy three-fold hollow sites, from which they desorb at T > 450 K. Note also, that in the low coverage regime (< 0.33 ML), the desorption peak shifts to a *lower* temperature at

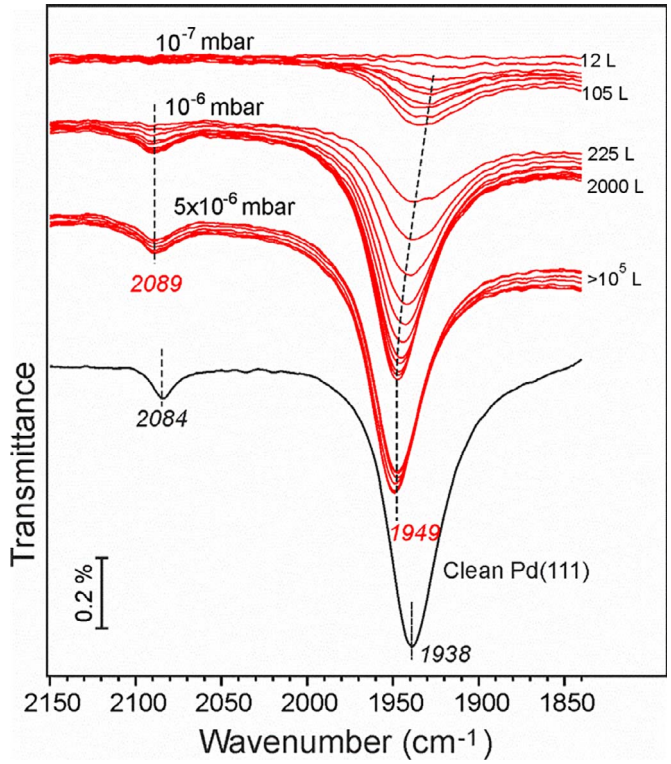

Fig. 3. Consecutive IRA spectra measured on a closed SiO_2/Pd(111) film at room temperature in CO atmosphere at pressures as indicated. The spectra are offset for clarity. The total CO exposures (in L) are shown close to the spectra. The spectrum for the clean Pd (111) surface exposed to 10 L is also shown for comparison.

increasing coverage, i.e. in contrast to the shift to a *higher* temperature observed here for silica-covered Pd(111) (Fig. 4). In the same manner as rationalized for Ru(0001)-supported films, the shift is most likely caused by the time needed for CO molecules underneath the film to find an appropriate pore to escape. Following the above description for CO desorption from the clean Pd(111) surface, the prominent signal at ~ 425 K can be assigned to CO desorbing primarily from the bridge sites, thus suggesting that the three-fold hollow sites are either not available (e.g. blocked) or not favorable for CO ad-species underneath the film. On the other hand, our DFT calculations show that the hollow sites are always preferred, from low to high CO coverage (see below). Thus, one has to assume that CO adsorption site redistribution (from the bridge to

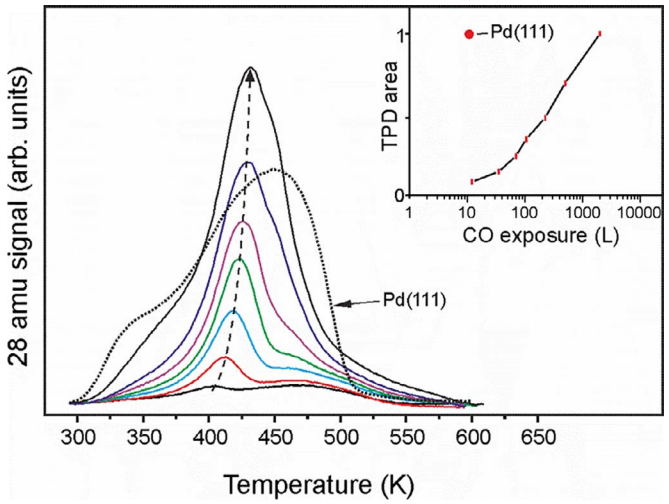

Fig. 4. TPD spectra measured on a fully covered silicate film at increasing CO dosage at 300 K. The spectrum for clean Pd(111) after exposure to 10 L is shown for comparison. Inset shows TPD area as a function of CO exposure.

the hollow), which occurs during TPD on pristine Pd(111), is hampered underneath the film.

The films were further studied with respect to D_2 adsorption. Fig. 5 displays a series of TPD spectra recorded upon various D_2 exposures at 1×10^{-7} mbar on the sample kept at 250 K. The adsorption temperature was chosen as a compromise to minimize D migration into the Pd (111) bulk that strongly affects the desorption spectra, [33] on the one hand, and to ease D_2 intercalation at the interface, on the other. For direct comparison, we show a spectrum obtained on the clean Pd(111) surface upon saturation, already reached at ~ 1 L. In contrast to Pd (111), D_2 desorbs from SiO_2/Pd(111) within an asymmetric signal centered at 330 K. The intensity scales with increasing dosage, although not linearly, apparently approaching saturation. Although the desorption occurs in the same temperature range as observed on the clean Pd(111) surface, there are, again, some differences between the two systems. The D_2 uptake on the silicate covered surface is remarkably, e.g. by a factor of 2, smaller than on the clean Pd. In principle, this coverage effect could explain a 35 K difference (330 vs 295 K) in peak positions since desorption maximum on Pd(111) shifts to low

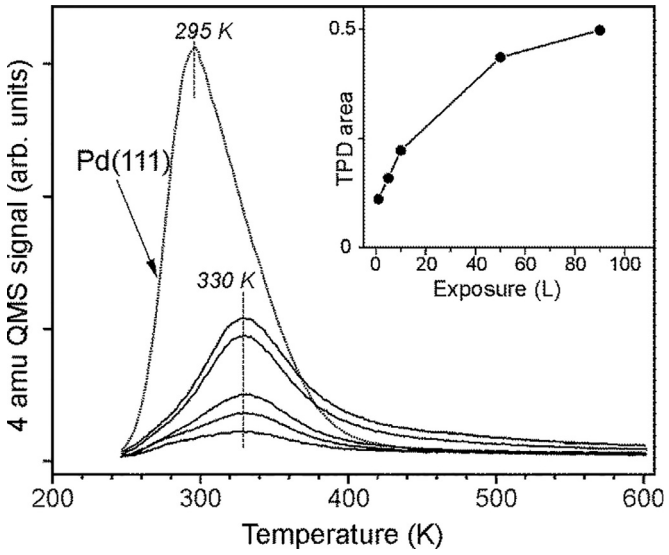

Fig. 5. TPD spectra of D_2 on SiO_2/Pd(111) as a function of exposure (in 1×10^{-7} mbar) at 250 K. The spectrum obtained by 1 L D_2 adsorption on clean Pd(111) is shown for comparison. The inset shows TPD signal areas, normalized to that on clean Pd(111).

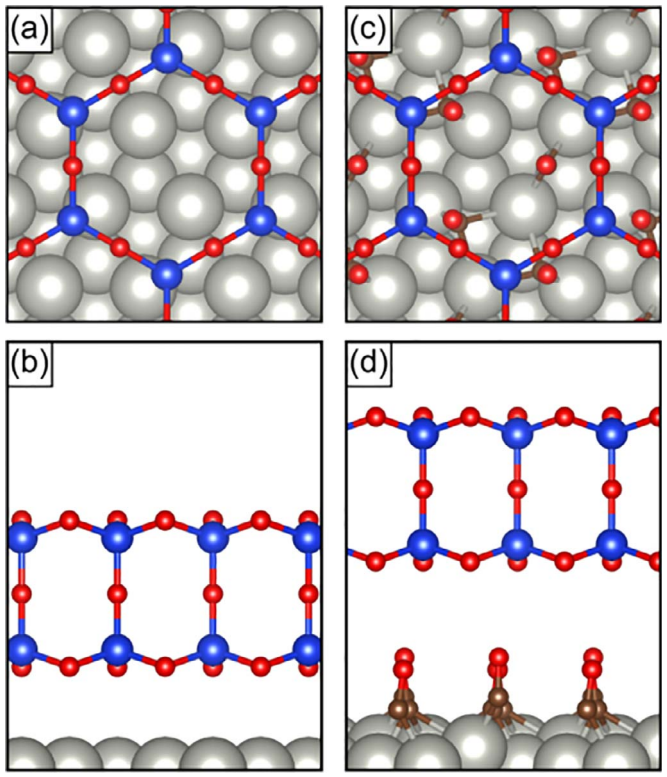

Fig. 6. Top and side views of silica bilayer supported on clean Pd(111) (a,b) and 3CO (2 × 2)-Pd(111) surfaces (c,d). Si atoms are blue, O - red, C - brown. (For interpretation of the colour code, please refer to the web-version of the article.)

temperatures at increasing coverages following 2-nd order desorption kinetics [33]. On the other hand, the coverage dependent shift is not observed on SiO_2/Pd(111). Together with a prominent desorption "tail" extending to higher temperatures, both findings indicate the desorption process that involves D_2 surface diffusion underneath the film in order to find a large pore to escape. Interestingly, on the Ru(0001)-supported films, the D_2 uptake correlates well with the CO uptake measured on the same sample [12]. Both CO and D_2 uptakes at saturation were equally (by ~ 35%) lower than on clean Ru(0001). Substantial difference between CO and D_2 uptakes observed here on Pd(111)-supported films may be explained by migration of D ad-atoms, which would otherwise desorb as D_2 from the uncovered surface, into the Pd bulk, thus reducing the total amount of D_2 desorbing.

3.2. Computational results

The DFT-optimized geometry of the crystalline silica bilayer on the Pd(111) surface (Fig. 6(a and b)) revealed that the center of the silica hexagon is located above a bridge Pd-Pd site. The distance between the Pd surface layer and the bottom O layer in silica is 3.0 Å. The film binds via dispersion forces as the adhesion energy only yields ~ 15 meV/nm^2. The silica bilayer reduces the work function by 0.39 eV as compared to the clean Pd(111) surface. About 10% of the work function change is caused by the compressive effect [34].

To validate the applied approach to CO adsorption, we first computed CO ad-layers on the clean Pd(111) surface. At low coverage (0.25 ML), CO adsorbs on 3-fold hollow sites, either fcc or hcp, since the corresponding adsorption energies are very close (−2.17 and −2.15 eV, for the hcp and fcc sites, respectively). These are considerably higher than on the top sites (−1.63 eV), in full agreement with the previous DFT studies [35,36]. In the presence of the silica bilayer, the adsorption energies are slightly reduced. The reduction is smallest for the bridge site (ΔE = 0.23 eV) and largest (0.36 eV) for CO on the top sites (Table 1). Thus, the hollow site remains preferred on

Table 1
Adsorption energies E_{ads} (in eV) of 0.25 ML CO on Pd(111) and SiO_2/Pd(111).

	Pd(111)	SiO_2/Pd(111)
top	−1.63	−1.27
bridge	−1.98	−1.75
fcc	−2.15	−1.84
hcp	−2.17	−1.91

Table 2
Adsorption energy E_{ads} (in eV) per CO molecule adsorbed in 3-fold hollow sites on Pd (111) and SiO_2/Pd(111).

Coverage (ML)	0.25	0.50	0.75
Pd	−2.17	−1.87	−1.59
SiO_2/Pd	−1.91	−1.73	−1.51
ΔE_{ads}	0.26	0.14	0.08

SiO_2/Pd(111) at low coverages.

The silica film affects the adsorption energy and hence the desorption temperatures for bridge and hollow sites in a different way due to steric effects: The difference in CO adsorption energies of bridge and hcp sites ranges from 0.19 eV on Pd(111) to 0.16 eV on SiO_2/Pd(111), see Table 1. Even larger is the difference between top and bridge sites, which is of 0.35 eV on Pd(111), but becomes 0.48 eV on SiO_2/Pd(111).

Also at higher CO coverages (0.5 and 0.75 ML), the hollow sites on Pd(111) are still most favorable, although the adsorption energy per CO molecule decreases with increasing coverage (Table 2), i.e. from −2.17 eV (0.25 ML), to −1.87 eV (0.5 ML), and to −1.59 eV (0.75 ML). The adsorption energies for CO underneath the silica follow the same trend and are −1.91, −1.73, and −1.51 eV, respectively. Accordingly, the differences in adsorption energies between clean and silica covered Pd(111) become smaller at high coverages. Note that, upon intercalation of 0.75 ML CO in the 3CO(2 × 2) structure, the interfacial silica-metal distance is increased from 3.0 to ~ 6.0 Å.

We have carefully checked the stability of CO on top sites by considering increasing CO coverages (0.5, 0.75, and 1 ML) with the molecules distributed in various positions, including situations where all the CO molecules occupy top sites. However, the result is that either the CO molecules move from top to bridge or from top to hollow sites or, when the CO molecules remain in top sites, the corresponding structures represent local minima on the potential energy surface, and are less stable than other arrangements where all CO molecules are in bridge or hollow positions.

In the next step, we examined the vibrational properties of CO. The scaling factor (1.008) was determined from comparison of calculated and experimental values of CO in the gas phase. The scaled frequencies computed for 0.25 ML CO on top, bridge and hcp sites are shown in Table 3. Note that the GGA approach is known to underestimate the HOMO-LUMO gap in CO, thus resulting in an excess of back-donation from the metal 2π* molecular orbital (MO) and hence in an overestimate of the red-shift of the CO frequency. Bearing in mind considerable data scattering in experimental results reported in the literature which is partially due to the fact that the frequencies depend on adsorption temperature and CO coverage [29,37–39], the results are in fairly good agreement with experiment.

Table 3
Stretching frequencies (in cm^{-1}) of CO on Pd(111) at 0.25 ML coverage.

CO position	top	hcp	bridge
DFT[a]	2074	1825	1903
Experiment[b]	2084 −2110	1823–1895	1920–1970

[a] Scaling factor is 1.008.
[b] From refs. [29,30,37,39]

Table 4
Scaled CO stretching frequencies (in cm^{-1}) computed for the 3CO-(2 × 2) ad-layer structure on clean and silica covered Pd(111).

SiO_2/Pd(111)	Pd(111)
2002	2002
1904	1904
1871	1872

To mimic only the situation at high coverages and to compare with IRAS results shown in Fig. 3, we used in the calculations the 3CO-(2 × 2) ad-layer structure (0.75 ML coverage). The presence of CO at the interface further reduces the adhesion energy of the silica layer, from 15 to 4.9 meV/nm^2. From the three CO molecules in the Pd(111)-(2 × 2) cell, one CO molecule sits over the bridge site whereas two occupy "atop" sites, see Fig. 6(c-d). Thus, at this coverage also atop sites become populated.

Actually, the "atop" site corresponds to a CO molecule slightly displaced towards the hollow site. Thus, even at this relatively high coverage (0.75 ML), we do not see CO occupying the Pd top sites. This can be due to the above-mentioned tendency of GGA calculations to overestimate the charge back-donation into the 2π* MO which favors a higher coordination of the CO molecule and adsorption on open sites. The computed scaled frequencies for the supercell considered are thus 1872, 1904, and 2002 cm^{-1} on both, Pd(111) and SiO_2/Pd(111) surfaces (Table 4). The mode at ~ 2002 cm^{-1} corresponds to an in-phase vibration of all three molecules normal to the Pd surface. The mode at ~ 1904 cm^{-1} corresponds to an in-phase vibration of the two CO molecules located at the "atop" sites and simultaneous anti-phase vibration of the CO molecule located at the bridge site. Finally, the mode at ~ 1870 cm^{-1} corresponds to the two atop CO molecules vibrating in anti-phase to each other. Thus, with this model we cannot account for the weak band observed at 2089 cm^{-1} in the experiment, and attributed to CO adsorbed on atop sites. We conclude that CO can occupy the atop positions only at low temperatures and high coverages.

Certainly, the calculations have been performed solely on crystalline silica overlayer, whereas the films exhibit a broad distribution of N-members silica rings and thus affecting the site occupation. Nonetheless, the DFT results show that while there is a moderate effect of the silica layer on the strength of the CO adsorption on the Pd(111) surface, the vibrational properties are hardly changed when the CO molecules are adsorbed underneath the SiO_2 film, in good agreement with experimental results shown in Figs. 3 and 4.

4. Conclusions

Ultrathin silicate films were successfully grown on Pd(111) using Si deposition onto O-pre-covered Pd(111) surface and subsequent oxidation at relatively mild temperatures (1000 – 1100 K). Similar to the case of a Pt(111) substrate, which is a more noble and in addition exhibits a larger lattice mismatch to the silicate layer, ultrathin silica films on Pd (111) grow exclusively as a bilayer film from the onset. Comparison with silicate films on Ru(0001) suggests that the affinity of a metal substrate to oxygen probably plays the decisive role as to whether the film grows as a mono- or bi-layer, while the lattice mismatch determines the crystallinity in the bilayer films. Thus both those factors have to be considered as descriptors in the growth of the silicate films on metals.

IRAS and TPD studies of CO and D_2 adsorption on the dense silicate films showed that both molecules penetrate the film, most likely through the largest pores available, and chemisorb on the Pd(111) surface. DFT calculations performed for a crystalline film show that the presence of the silica bilayer has little effect on the CO stretching frequencies, but results in a moderate reduction of the CO binding energy,

in full agreement with the experimental observation. This effect can be important for the reactivity of the molecular species adsorbed below the silica film. Overall, we believe that the study provides a further step in our understanding of adsorption and reactions in confined space provided by the interface.

Certainly, a full description of the reaction network activated upon film exposure to ambient gases, which includes gas permeation, diffusion of ad-species and reactions on the metal surface underneath the film as well as subsequent desorption of products, is in need of an adequate kinetic model. However, a number of diffusion channels across the surface and through the silica film should be investigated at the DFT level before one will be able to propose such a model. This information is missing, and the work is in progress currently.

Acknowledgments

We acknowledge financial support by Fonds der Chemischen Industrie and German-Israeli Foundation (Grant I-81-302.11-2013). GP thanks the Italian MIUR for the support through the PRIN Project 2015K7FZLH SMARTNESS “Solar driven chemistry: new materials for photo– and electro–catalysis”.

References

[1] S. Shaikhutdinov, H.-J. Freund, Ultrathin silica films on metals: the long and winding road to understanding the atomic structure, Adv. Mater. 25 (2013) 49–67.
[2] X. Xu, D.W. Goodman, New approach to the preparation of ultrathin silicon dioxide films at low temperatures, Appl. Phys. Lett. 61 (1992) 774–776.
[3] E.I. Altman, J. Götzen, N. Samudrala, U.D. Schwarz, Growth and characterization of crystalline silica films on Pd(100), J. Phys. Chem. C 117 (2013) 26144–26155.
[4] J. Weissenrieder, S. Kaya, J.L. Lu, H.J. Gao, S. Shaikhutdinov, H.J. Freund, M. Sierka, T.K. Todorova, J. Sauer, Atomic structure of a thin silica film on a Mo (112) substrate: a two-dimensional network of SiO_4 Tetrahedra, Phys. Rev. Lett. 95 (2005) 076103.
[5] X. Yu, B. Yang, J.A. Boscoboinik, S. Shaikhutdinov, H.-J. Freund, Support effects on the atomic structure of ultrathin silica films on metals, Appl. Phys. Lett. 100 (2012) 151608-151604.
[6] D. Löffler, J.J. Uhlrich, M. Baron, B. Yang, X. Yu, L. Lichtenstein, L. Heinke, C. Büchner, M. Heyde, S. Shaikhutdinov, H.J. Freund, R. Włodarczyk, M. Sierka, J. Sauer, Growth and structure of crystalline silica sheet on Ru(0001), Phys. Rev. Lett. 105 (2010) 146104.
[7] S. Shaikhutdinov, H.J. Freund, Ultra-thin silicate films on metals, J. Phys. 27 (2015) 443001.
[8] M. Heyde, S. Shaikhutdinov, H.J. Freund, Two-dimensional silica: Crystalline and vitreous, Chem. Phys. Lett. 550 (2012) 1–7.
[9] L. Lichtenstein, M. Heyde, H.-J. Freund, Crystalline-vitreous interface in two dimensional silica, Phys. Rev. Lett. 109 (2012) 106101.
[10] L. Lichtenstein, C. Büchner, B. Yang, S. Shaikhutdinov, M. Heyde, M. Sierka, R. Włodarczyk, J. Sauer, H.-J. Freund, The atomic structure of a metal-supported vitreous thin silica film, Angewandte Chemie International Edition 51 (2012) 404–407.
[11] A. Malashevich, S. Ismail-Beigi, E.I. Altman, Directing the structure of two-dimensional silica and silicates, J. Phys. Chem. C 120 (2016) 26770–26781.
[12] E. Emmez, B. Yang, S. Shaikhutdinov, H.-J. Freund, Permeation of a single-layer SiO_2 membrane and chemistry in confined space, J. Phys. Chem. C 118 (2014) 29034–29042.
[13] E. Emmez, J. Anibal Boscoboinik, S. Tenney, P. Sutter, S. Shaikhutdinov, H.-J. Freund, Oxidation of the Ru(0001) surface covered by weakly bound, ultrathin silicate films, Surface Sci. 646 (2016) 19–25.
[14] P. Sutter, J.T. Sadowski, E.A. Sutter, Chemistry under cover: tuning metal−-graphene interaction by reactive intercalation, J. Am. Chem. Soc. 132 (2010) 8175–8179.
[15] Y. Yao, Q. Fu, Y.Y. Zhang, X. Weng, H. Li, M. Chen, L. Jin, A. Dong, R. Mu, P. Jiang, L. Liu, H. Bluhm, Z. Liu, S.B. Zhang, X. Bao, Graphene cover-promoted metal-catalyzed reactions, Proc. Natl. Acad. Sci. USA 111 (2014) 17023–17028.
[16] J.-H. Jhang, C. Zhou, O.E. Dagdeviren, G.S. Hutchings, U.D. Schwarz, E.I. Altman, Growth of two dimensional silica and aluminosilicate bilayers on Pd(111): from incommensurate to commensurate crystalline, Phys. Chem. Chem. Phys. 19 (2017) 14001–14011.
[17] G. Kresse, J. Hafner, Ab initio, Phys. Rev. B 47 (1993) 558–561.
[18] G. Kresse, J. Hafner, Ab initio, Phys. Rev. B 49 (1994) 14251–14269.
[19] G. Kresse, J. Furthmüller, Efficiency of ab-initio total energy calculations for metals and semiconductors using a plane-wave basis set, Comput. Mater. Sci. 6 (1996) 15–50.
[20] G. Kresse, J. Furthmüller, Efficient iterative schemes for ab initio total-energy calculations using a plane-wave basis set, Phys. Rev. B 54 (1996) 11169–11186.
[21] J.P. Perdew, K. Burke, M. Ernzerhof, Generalized gradient approximation made simple, Phys. Rev. Lett. 77 (1996) 3865 Physical Review Letters, 78 (1997) 1396-1396.
[22] P.E. Blöchl, Projector augmented-wave method, Phys. Rev. B 50 (1994) 17953–17979.
[23] G. Kresse, D. Joubert, From ultrasoft pseudopotentials to the projector augmented-wave method, Phys. Rev. B 59 (1999) 1758–1775.
[24] H.J. Monkhorst, J.D. Pack, Special points for Brillouin-zone integrations, Phys. Rev. B 13 (1976) 5188–5192.
[25] S. Tosoni, J. Sauer, Accurate quantum chemical energies for the interaction of hydrocarbons with oxide surfaces: CH_4/MgO(001), Phys. Chem. Chem. Phys. 12 (2010) 14330–14340.
[26] C.N.R. Rao, P.V. Kamath, S. Yashonath, Molecularly adsorbed oxygen on metals: electron spectroscopic studies, Chem. Phys. Lett. 88 (1982) 13–16.
[27] B. Yang, W.E. Kaden, X. Yu, J.A. Boscoboinik, Y. Martynova, L. Lichtenstein, M. Heyde, M. Sterrer, R. Wlodarczyk, M. Sierka, J. Sauer, S. Shaikhutdinov, H.-J. Freund, Thin silica films on Ru(0001): monolayer, bilayer and three-dimensional networks of [SiO_4] tetrahedra, Phys. Chem. Chem. Phys. 14 (2012) 11344–11351.
[28] U. Martinez, L. Giordano, G. Pacchioni, Nature of point defects on SiO_2/Mo(112) thin films and their interaction with Au atoms, J. Phys. Chem. B 110 (2006) 17015–17023.
[29] W.K. Kuhn, J. Szanyi, D.W. Goodman, CO adsorption on Pd(111): the effects of temperature and pressure, Surface Sci. 274 (1992) L611–L618.
[30] A.M. Bradshaw, F.M. Hoffmann, The chemisorption of carbon monoxide on palladium single crystal surfaces: IR spectroscopic evidence for localised site adsorption, Surface Sci. 72 (1978) 513–535.
[31] X. Guo, J.T. Yates, Dependence of effective desorption kinetic parameters on surface coverage and adsorption temperature: CO on Pd(111), J. Chem. Phys. 90 (1989) 6761–6766.
[32] P. Schlexer, G. Pacchioni, R. Włodarczyk, J. Sauer, CO adsorption on a silica bilayer supported on Ru(0001), Surface Sci. 648 (2016) 2–9.
[33] G.E. Gdowski, T.E. Felter, R.H. Stulen, Effect of surface temperature on the sorption of hydrogen by Pd(111), Surface Sci. 181 (1987) L147–L155.
[34] L. Giordano, G. Pacchioni, Oxide films at the nanoscale: new structures, new functions, and new materials, Accounts Chem. Res. 44 (2011) 1244–1252.
[35] D. Loffreda, D. Simon, P. Sautet, Dependence of stretching frequency on surface coverage and adsorbate–adsorbate interactions: a density-functional theory approach of CO on Pd (111), Surface Sci. 425 (1999) 68–80.
[36] G.W. Watson, R.P.K. Wells, D.J. Willock, G.J. Hutchings, A comparison of the adsorption and diffusion of hydrogen on the {111} surfaces of Ni, Pd, and Pt from density functional theory calculations, J. Phys. Chemistry B 105 (2001) 4889–4894.
[37] B. Bourguignon, S. Carrez, B. Dragnea, H. Dubost, Vibrational spectroscopy of imperfect CO/Pd(111) surfaces obtained by adsorption between 150 and 230 K, Surface Sci. 418 (1998) 171–180.
[38] M. Tüshaus, W. Berndt, H. Conrad, A.M. Bradshaw, B. Persson, Understanding the structure of high coverage CO adlayers, Appl. Phys. A 51 (1990) 91–98.
[39] T. Dellwig, G. Rupprechter, H. Unterhalt, H.J. Freund, Bridging the pressure and materials gaps: high pressure sum frequency generation study on supported pd nanoparticles, Phys. Rev. Letters 85 (2000) 776–779.